Constraining the Nuclear Equation of State at Subsaturation Densities

E. Khan,[1] J. Margueron,[1] and I. Vidaña[2]

[1]*Institut de Physique Nucléaire, Université Paris-Sud, IN2P3-CNRS, F-91406 Orsay Cedex, France*

[2]*Centro de Física Computacional, Department of Physics, University of Coimbra, PT-3004-516 Coimbra, Portugal*

(Received 22 November 2011; revised manuscript received 27 March 2012; published 27 August 2012)

Only one-third of the nucleons in ^{208}Pb occupy the saturation density area. Consequently, nuclear observables related to the average properties of nuclei, such as masses or radii, constrain the equation of state not at the saturation density but rather around the so-called crossing density, localized close to the mean value of the density of nuclei: $\rho \simeq 0.11$ fm^{-3}. This provides an explanation for the empirical fact that several equation of state quantities calculated with various functionals cross at a density significantly lower than the saturation one. The third derivative M of the energy per unit of volume at the crossing density is constrained by the giant monopole resonance measurements in an isotopic chain rather than the incompressibility at saturation density. The giant monopole resonance measurements provide $M = 1100 \pm 70$ MeV (6% uncertainty), whose extrapolation gives $K_\infty = 230 \pm 40$ MeV (17% uncertainty).

DOI: 10.1103/PhysRevLett.109.092501 PACS numbers: 21.10.Re, 21.65.−f, 21.60.Jz

Constraining the nuclear equation of state (EOS) and reducing the uncertainties on nuclear matter properties in dense stellar objects such as neutron stars and supernovae is one of the major goals of nuclear physics. To do so observables such as masses, radii or energy centroid of the isoscalar giant monopole resonance (GMR) are measured in finite nuclei. Relating the EOS to such observables is usually undertaken in several ways. The liquid drop expansion [1] is one of the most used methods. In its generalized version, one performs a development of a quantity (the mass for instance) considered at saturation density (volume term), adding several terms such as the surface one. It should be noted that taking the volume term at saturation density is based on the fact that the inner part of the nuclei density is close to the saturation. Another method is the so-called local density approximation [2]. In this approach the global properties in nuclei are obtained from considering nuclei as local pieces of nuclear matter. Finally, another method is based on the microscopic approach, relying on energy density functionals (EDF): using various EDFs, a correlation diagram is drawn between the predicted observable and a related property of the EOS. The measurement of the observable allows the validation of EDF and the corresponding property of the EOS [3–6]. For instance, the neutrons skin measurement is correlated with the slope of the symmetry energy. It should be noted that usually EDF are designed using masses, radii but also the nuclear incompressibility [7,8].

Each of these methods comprise, however, limitations. The liquid drop expansion is known not to be accurate enough in the case of the incompressibility at the saturation density [9,10], although the inclusion of higher other terms is relevant [11]. The liquid drop expansion of the mass has been successful, providing an accurate determination of the saturation energy. This quantity is now used in EDF determination, but this is an exceptional case, related to the profusion of data available on masses. In the case of the local density approximation, its validity is generally questionable for finite size systems. Finally, in the case of the microscopic approach, the EDF employed has usually been adjusted to data on magic nuclei, whereas most applications are aimed to be used for deformed open-shell nuclei. However, there may be a general consensus that the microscopic approach should be used in fine, because of its accuracy and reliability.

It seems for now difficult to straightforwardly determine the nuclear incompressibility even with the microscopic method. The earliest microscopic analysis came to a value of $K_\infty = 210$ MeV [9], but with the advent of microscopic relativistic approaches, a value of $K_\infty = 260$ MeV was obtained [12]. It has been shown that this value is not determined accurately and that the density dependence of the EDF as well as pairing effects (and, therefore, the shell structure) have an impact on the determination of K_∞ [13–15]. Using K_∞ in the design of EDF may not be a sound approach since it cannot be safely determined by the microscopic method. Therefore, the method of determination of the nuclear incompressibility has to be rethought and more generally, it is necessary to clarify the link between nuclear matter EOS determination and nuclear observables.

First, it should be noted that the liquid drop expansion is not a perturbative one since the surface properties of the nucleus are almost as important as the bulk one. Hence, it may be a misleading idea to consider the nucleus as mainly composed of nucleons at saturation density with a few at the surface. Let us consider the case of ^{208}Pb which is usually considered as a benchmark for extracting bulk properties. Figure 1 shows the total density calculated in the Skyrme Hartree-Fock (HF) approach. The lower part shows the usual representation of the density whereas the upper part displays an equivalent representation with an

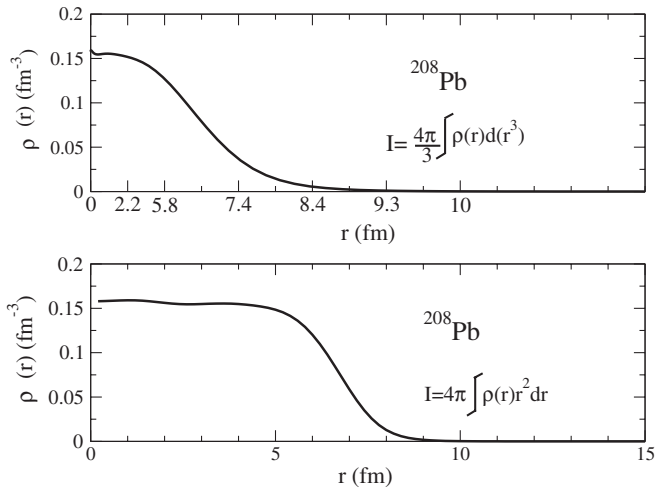

FIG. 1. Matter density of ^{208}Pb calculated with the HF approach using the SLy4 functional with different X axis scales. Top: representation taking into account the nucleons' distribution in the nucleus. Bottom: usual representation.

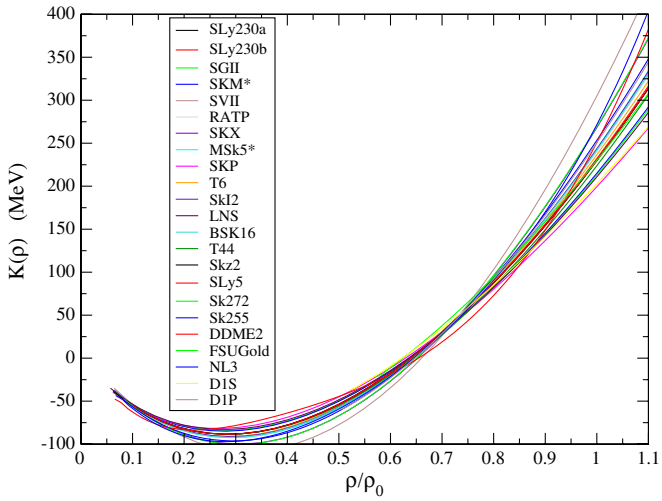

FIG. 2 (color online). EOS incompressibility calculated with various functionals, showing the crossing density around $0.7\rho_0 \simeq 0.11$ fm^{-3}.

X axis scaled as r^3. This allows taking into account the increase of nucleons per volume unit; the total number of nucleons corresponds to the integral of constant steps of the radial density represented on the upper part of Fig. 1. It is now perceptible that about one-third of the nucleons of the ^{208}Pb nucleus lie in the saturation density area, whereas two-thirds are localized in the surface at a density lower than the saturation one. Therefore, even in heavy nuclei, the contribution of the surface is larger with respect to the volume one, raising the question of the legitimacy of constraining EOS quantities at saturation density by measurements of nuclear observables.

Another illustration is given by calculating the mean density of the ^{208}Pb nucleus. Using a Skyrme-HF calculation, one obtains $\langle\rho\rangle = 0.12$ fm^{-3} in ^{208}Pb with a variance $\sqrt{\langle\rho^2\rangle - \langle\rho^2\rangle} = 0.04$ fm^{-3}. Therefore, the density value characterizing a nucleus is not the saturation one ($\rho_0 = 0.16$ fm^{-3}) but a significantly lower one, with a range spanning from $\rho_0/2$ to ρ_0. It should be noted that the dependence of the mean density on the nucleus is rather weak: 0.11 fm^{-3} for ^{120}Sn. In light nuclei, the mean density drops down as expected: 0.07 fm^{-3} for ^{40}Ca.

Consequently, the measurement of an averaged observable in a nucleus is more properly related to a correlated EOS quantity defined around the mean density than at the saturation density. This fact is illustrated on Fig. 2, where the density-dependent incompressibility, defined by [16,17]

$$K(\rho) = \frac{9}{\rho\chi(\rho)} = 9\rho^2 \frac{\partial^2 E(\rho)/A}{\partial\rho^2} + \frac{18}{\rho} P(\rho), \qquad (1)$$

and obtained from various EDFs is plotted with several Skyrme, Gogny and relativistic interactions, all designed to describe observables in nuclei such as masses and radii. They intersect around the crossing density $\rho_c \simeq 0.7\rho_0 \simeq 0.11$ fm^{-3}. The existence of a crossing density has been empirically noticed in previous works on the symmetry energy (Fig. 2 of Ref. [6]), pairing gap (Fig. 2 of Ref. [18]) or the neutron EOS (Fig. 2 of Ref. [3] and Fig.1 of Ref. [4]), and we provide here an explanation, related to the mean density: when designing EDF with nuclear observables, the corresponding EOS is constrained not at the saturation density but rather around the mean density (the crossing density). In the case of the symmetry energy, the value at a density $\rho \simeq 0.11$ fm^{-3} is taken to be around 25 MeV, a value close to the symmetry energy coefficient of the liquid drop expansion [5,6,19], as an empirical prescription. This last value contains both a volume and surface terms, and thus represents the symmetry energy extracted from nuclei observables. For the incompressibility, the GMR is known to be related to the mean square radius of the nucleus by the energy weighted sum rule [2]. In the design of EDFs, the considered constraint on nuclear radii induces a constraint on the compression mode, likely explaining the crossing around $0.7\rho_0$ observed on Fig. 2. This shows the universality of the crossing effect, arising from the constraints encoded in the EDF from nuclei observables. Due to this crossing area, a larger $K_\infty = K(\rho_0)$ value for a given EDF can be compensated by lower values of $K(\rho)$ at sub-crossing densities, so to predict a similar energy of the GMR in nuclei: the GMR centroid is related to the integral of $K(\rho)$ over a large density range [17]. This allows us to understand how EDF with different K_∞ can predict a similar energy of the GMR, as noted in Ref. [15].

Various EDF's shall exhibit various density dependencies around the crossing point. At first order the derivative of the incompressibility (or symmetry energy or pairing gap) at this point will differ between various EDF's. Complementary measurements in nuclei are needed to characterize these derivatives. For instance in Ref. [3,4]

the derivative of the neutron EOS around $\rho_c \simeq 0.11$ fm^{-3} is found to be constrained by neutron skin measurements in ^{208}Pb. The associated interpretation was that the 0.11 fm^{-3} density was considered as the neutron saturation density in nuclei. We provide an alternative and general view: 0.11 fm^{-3} corresponds to the crossing density, as seen on Fig. 2.

We apply this method to the determination of the nuclear incompressibility. When the giant monopole resonance is measured and well reproduced by a given EDF, it shall therefore not be correlated with the incompressibility of EOS at saturation density but rather with its first derivative M around the crossing density. It should be recalled that the crossing density exists because the EDF are determined by including nuclear observables such as masses and radii in their fit. On Fig. 2 the crossing point at $\rho_c \simeq 0.7\rho_0$ yields $K(\rho_c) \simeq 40$ MeV for the incompressibility (this is analogous to the fixed symmetry energy taken to be 25 MeV, as discussed above). To be consistent with a generalized liquid drop expansion [20], the derivative M of the incompressibility at this point is defined by:

$$M = 3\rho K'(\rho)|_{\rho=\rho_c}, \tag{2}$$

where $K'(\rho)$ is the derivative of the incompressibility density dependent term defined in Eq. (1).

Most of the GMR measurements have been performed on ^{208}Pb and data on other nuclei like the Sn isotopic chain is relevant [21]. In Fig. 3 the GMR prediction using the constrained Hartree-Fock (CHF) method as a function of M is shown for various Skyrme EDF's in ^{208}Pb and ^{120}Sn. The CHF method is a sum rule approach to calculate the centroid energy of the isoscalar GMR:

$$E_{\mathrm{ISGMR}} = \sqrt{\frac{m_1}{m_{-1}}}. \tag{3}$$

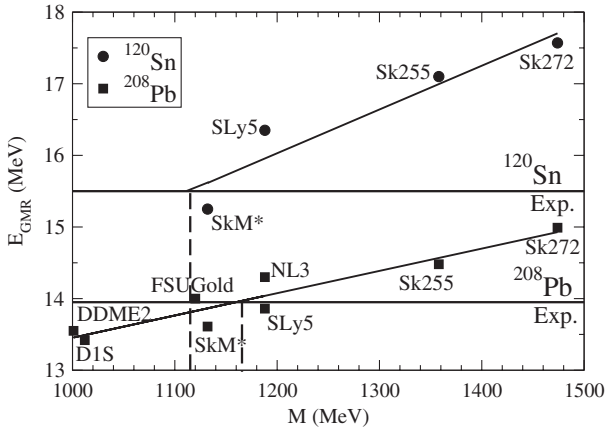

FIG. 3. Centroid of the GMR in ^{208}Pb and ^{120}Sn calculated with the CHF method vs the value of M for various functionals. The experimental values for ^{208}Pb and ^{120}Sn are taken from Refs. [21,27], respectively, with respective error bars of ± 200 and ± 100 keV.

The m_1 moment is evaluated by the double commutator using the Thouless theorem [2] and for the m_{-1} moment, the CHF approach is used [14,22,23]: the CHF Hamiltonian is built by adding the constraint associated with the IS monopole operator. The CHF method has the advantage to very precisely predict the centroid of the GMR using the m_{-1} sum rule. To be comprehensive, Fig. 3 also displays values for several relativistic and the Gogny D1S EDFs in the case of ^{208}Pb.

The value of M deduced from both nuclei is compatible within few percents. In order to derive a sound value of M, we have further performed similar calculations in the $^{112-124}$Sn isotopes, as well as in ^{90}Zr and ^{144}Sm nuclei, leading to $M \simeq 1100$ MeV $\pm$ 70 MeV. The contributions to the uncertainty shall come from the small variance between the mean density in the respective nuclei compared to the crossing density, the isospin dependence of the incompressibility and the pairing effects. The linear correlation observed on Fig. 3 is striking, since the interactions employed can have a symmetry energy spanning from 30 to 37 MeV. This shows that the present results moderately depend on the isospin asymmetry of the system studied. The neutron vs proton asymmetry parameter $\delta = (N - Z)/A$ also remains rather constant in the considered nuclei for the GMR such as ^{208}Pb and stable Tin isotopes: $\delta \simeq 0.2$, validating the present isospin-independent approach.

It should be noted that the present method clarifies the issue of determining different incompressibility values at saturation when using either the Pb or the Sn data [14,24]: a close M value is found with these two data sets. However the remaining discrepancy of the M values deduced from the Sn and the Pb measurements shows that the proper density dependence of the EDFs has not been revealed yet. Another striking feature is that the Gogny and relativistic EDFs are found on the same linear correlation than the Skyrme one, showing the universality of the E_{GMR} vs M correlation, contrary to the E_{GMR} vs K_∞ one: it is well known that relativistic EDFs can predict a similar E_{GMR} in ^{208}Pb but with a significantly larger value of K_∞ [12].

Let us now investigate why a clear correlation exists between the centroid of the GMR and K_∞ in the specific case of the Skyrme functionals. [15]. Figure 4 displays the relative contribution of the kinetic, central (t_0), finite range (t_1, t_2) and density (t_3) terms of the Skyrme functionals to the EOS and its derivative values at the crossing density. A striking regularity is observed among the functionals used. The dominant terms are the central and the density ones, but the central term vanishes from the second derivative of the EOS and beyond, allowing the density term (in ρ^α) to dominate alone. Therefore, the second derivative terms and beyond are correlated to each other, implying that the correlation between M and E_{GMR} is propagated to the one between K_∞ and E_{GMR}: a linear correlation is preserved between M and K_∞ due to the vanishing of the

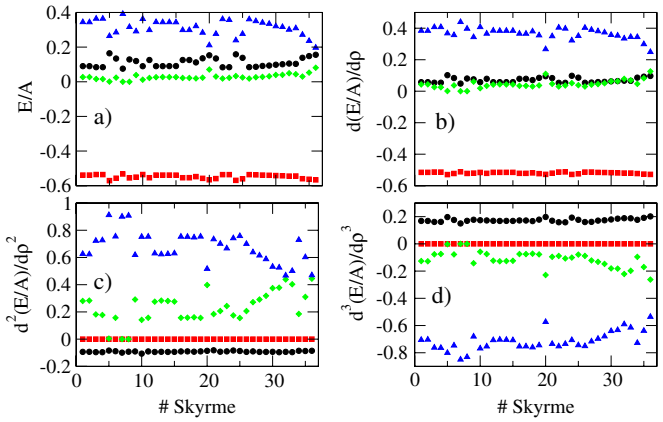

FIG. 4 (color online). Positive or negative relative contribution of the kinetic (circles), central (squares), finite range (diamonds) and density (triangles) terms to the equation of state (a), its first (b), second (c) and third (d) derivatives at the crossing density, calculated for 36 Skyrme functionals.

central term from the second derivative and beyond of the equation of state. In other words, the density dependence of the incompressibility, driven by these derivatives, is correlated to M. Therefore, K_∞ is correlated to M, and this outcome is similar for all Skyrme functionals as seen on Fig. 4: the (E_{GMR}, K_∞) linear correlation may be due to the similar form of the density dependence among the Skyrme EDFs.

But this linear correlation is deteriorated when including together both Skyrme and relativistic EDF predictions, as mentioned above. M shall be the exclusive quantity which can be deduced from GMR measurements, whereas the K_∞ determination relies on additional density dependence assumptions. Using the M value at the crossing point, a linear expansion provides $K_\infty = 230$ MeV. An uncertainty of ± 40 MeV can be inferred from the spreading of K_∞ values on Fig. 2 obtained with the various functionals, which is of the order of $\pm 17\%$. It is, therefore, argued that measurements in nuclei constrain the EOS around the crossing density (namely the derivative of the EOS quantity at the crossing density) and deducing values at saturation density remains a mainly model-dependent extrapolation. In the case of nuclear incompressibility, it is proposed to change the usual E_{GMR} vs K_∞ correlation plot and to replace it by a more reliable and universal E_{GMR} vs M plot (Fig. 3), where M is the derivative of the incompressibility at the crossing density. The measurement of the GMR in more neutron-rich nuclei [25,26] will certainly open the possibility to study a part of the isospin dependence of the incompressibility.

This work has been partly supported by the ANR NExEN and SN2NS contracts, the Institut Universitaire de France, by CompStar, a Research Networking Programme of the European Science Foundation, and by the initiative QREN financed by the UE/FEDER through the Programme COMPETE under the Projects No. PTDC/FIS/113292/2009, No. CERN/FP/109316/2009, and No. CERN/FP/116366/2010. J. M. would like to thank K. Bennaceur and J. Meyer for useful discussions during the completion of this work.

[1] C. F. Von Weizsäcker, Z. Phys.**96**, 431 (1935); H. A. Bethe and R. F. Bacher, Rev. Mod. Phys. **8**, 82 (1936).
[2] P. Ring and P. Schuck, *The Nuclear Many-Body Problem* (Springer-Verlag, Heidelberg, 1980).
[3] B. A. Brown, Phys. Rev. Lett. **85**, 5296 (2000).
[4] S. Typel and B. A. Brown, Phys. Rev. C **64**, 027302 (2001).
[5] M. Centelles, X. Roca-Maza, X. Viñas, and M. Warda, Phys. Rev. Lett. **102**, 122502 (2009).
[6] J. Piekarewicz, Phys. Rev. C **83**, 034319 (2011).
[7] M. Bender, P.-H. Heenen, and P.-G. Reinhard, Rev. Mod. Phys. **75**, 121 (2003).
[8] D. Lunney, J. M. Pearson, and C. Thibault, Rev. Mod. Phys. **75**, 1021 (2003).
[9] J.-P. Blaizot, Phys. Rep. **64**, 171 (1980).
[10] J. M. Pearson, Phys. Lett. B **271**, 12 (1991).
[11] S. K. Patra, M. Centelles, X. Viñas and M. Del Estal, Phys. Rev. C **65**, 044304 (2002).
[12] D. Vretenar, T. Niksic, and P. Ring, Phys. Rev. C **68**, 024310 (2003).
[13] J. Li, G. Colò, and J. Meng, Phys. Rev. C **78**, 064304 (2008).
[14] E. Khan, Phys. Rev. C **80**, 011307(R) (2009).
[15] G. Colò, N. V. Giai, J. Meyer, K. Bennaceur, and P. Bonche, Phys. Rev. C **70**, 024307 (2004).
[16] A. L. Fetter and J. D. Walecka, *Quantum Theory of Many-Particle Systems* (McGraw-Hill, New York, 1971).
[17] E. Khan, J. Margueron, G. Colò, K. Hagino, and H. Sagawa, Phys. Rev. C **82**, 024322 (2010).
[18] E. Khan, M. Grasso, and J. Margueron, Phys. Rev. C **80**, 044328 (2009).
[19] C. J. Horowitz and J. Piekarewicz, Phys. Rev. Lett. **86**, 5647 (2001).
[20] C. Ducoin, J. Margueron, C. Providência, and I. Vidaña, Phys. Rev. C **83**, 045810 (2011).
[21] T. Li *et al.*, Phys. Rev. Lett. **99**, 162503 (2007).
[22] O. Bohigas, A. M. Lane, and J. Martorell, Phys. Rep. **51**, 267 (1979).
[23] L. Capelli, G. Colò, and J. Li, Phys. Rev. C **79**, 054329 (2009).
[24] J. Piekarewicz, Phys. Rev. C **76**, 031301 (2007).
[25] C. Monrozeau *et al.*, Phys. Rev. Lett. **100**, 042501 (2008).
[26] M. Vandebrouck *et al.*, Exp. E456a GANIL (2010).
[27] D. H. Youngblood, Y.-W. Lui, H. L. Clark, B. John, Y. Tokimoto, and X. Chen, Phys. Rev. C **69**, 034315 (2004).